Reliability and Vulnerability Studies of the SP-100 Dual-Loop Thermoelectric-Electromagnetic Pump

Mohamed S. El-Genk* and William J. Rider†
University of New Mexico, Albuquerque, New Mexico 87131

This research has developed a transient model of the dual-loop thermoelectric-electromagnetic pump of the SP-100 space nuclear power system and performed a parametric analysis assessing the reliability and vulnerability of the pump to overheating of the secondary coolant. Results show that the pump ceases to operate when the secondary coolant temperature either equals that of the primary coolant or exceeds 1255 K, regardless of the value of the primary coolant temperature. In any case, increasing the secondary coolant temperature degrades the SP-100 pump performance through both reducing the electric current produced by the thermoelectric generators and the magnetic flux of the pump. Because the SP-100 pump employs a self-induced magnet at secondary coolant temperatures lower than 1255 K but higher than the primary coolant temperature, the pump maintains forward operation because both the electric current and the magnetic field reverse direction. However, had the SP-100 pump been designed with a permanent magnet, raising the secondary coolant temperature beyond that of the primary coolant temperature would only reverse the electric current, causing the pump to operate in reverse. Results also show that although insulating the pump's magnetic structure from the secondary coolant ducts insignificantly affects the steady-state nominal operation of the pump, it improves pump performance and reduces the pump's vulnerability to external heating of the secondary coolant to temperatures in excess of 1000 K.

Nomenclature

A = surface or cross-sectional area, m^2
a = pump duct height or insulation foil thickness, m
B = magnetic field, G
b = pump duct width, m
Cp = specific heat, J/kg K
D_e = equivalent hydraulic diameter, m
E = electric potential across the pump duct, V
E_i = counter EMF induced in the liquid metal flowing through the pump duct and intersecting the magnetic field lines, V
F = radiator view factor
H = heat-transfer coefficient, W/m^2
I = electric current, A
k = thermal conductivity, W/m K
L = length of the pump, m
M = mass, kg
N = number of insulation foils or number of coolant ducts
P = power, W
Pe = Peclet number
Q = coolant volumetric flow rate, m^3/s
R,r = electrical resistance, Ω
T = temperature, K
t = time, s
x = wall thickness, m
ΔP = pressure head, Pa
ϵ = surface emissivity
η = efficiency
ρ = density, kg/m^3
σ = Stefan-Boltzmann constant, 5.669×10^{-8} $W/m^2 K^4$

Subscripts

Al = alumina insulation
a = ambient
av = average
B = upper electric bus
c = coolant
EM = electromagnetic
e = effective or electric
f = fringe or fluid
foil = insulation foil region
g_1 = gap between the alumina insulation and the magnetic structure
g_2 = gap between the alumina structure and the upper electric bus
i = magnetic structure or electric bus
loss = thermal losses to the magnet
M = mechanical
m = magnetic structure or between the magnetic structure and auxiliary radiator
o = initial
p = primary coolant or primary duct
r = auxiliary radiator
s = secondary coolant or duct
s_1 = secondary duct to magnet
s_2 = secondary duct to upper electric bus
TE = thermoelectric
TE-EM = thermoelectric-electromagnetic
t = thermal
W = duct walls normal to the flow of electric current
w = duct walls parallel to the flow of electric current
wm = duct wall material

Received Aug. 25, 1988; revision received Jan. 5, 1989.

*Professor and Director of the Institute for Space Nuclear Power Studies.

†Graduate Student, Department of Chemical and Nuclear Engineering.

Introduction

THE SP-100 space nuclear power program was established in February 1983 to develop and demonstrate the technology of a space nuclear power system in the range from 10 kW to 1 MW.[1] In the fall of 1985 the thermoelectric (TE) SP-100 concept of the General Electric Company was selected as the

baseline design for subsequent engineering development and testing.[2] A ground engineering test of the nuclear system is planned for early 1992, while a flight demonstration of the entire system is projected for 1995.

The SP-100 baseline design incorporates a 2.5-MW fast-flux lithium-cooled nuclear reactor with SiGe/GaP TE generators for partially converting the reactor thermal energy to electricity for a nominal system electric power of 100 kW. The remaining reactor thermal energy is transported by a pumped loop system referred to here as the secondary loops, to a potassium heat pipe radiator where the waste heat is rejected into space (see Figs. 1 and 2). However, since 1985 the SP-100 concept has undergone several design changes to enhance the reliability and safety of the system and reduce its mass. For example, to improve the redundancy of the reactor's cooling system, the latest design increased the number of parallel loops, referred to as the primary loops, from three in the early design to 12. Also, to reduce the overall mass of the system, the 4–6.5 m-long potassium heat pipes that transport waste heat for the power conversion assemblies (PCAs) to the radiator have been replaced with 12 liquid lithium secondary loops. Finally, for high relability and redundancy of the waste heat transport system, each secondary loop has been coupled to a separate but identical heat pipe radiator panel. Hence, a loss of coolant or flow in one of the secondary loops would not endanger the operation of the entire waste heat removal system.

As delineated in Fig. 2, each pair of the primary and secondary loops is thermally coupled in the PCA and thermal-hydraulically coupled in the thermoelectric-electromagnetic (TE-EM) pump. The coupling of the secondary and primary coolants in the pump alleviates the need for using a large radiator for rejecting the waste heat from the pump TE generators, which was the case in the early SP-100 design employing single-loop TE-EM pumps.[3,4] However, each dual-loop pump is equipped with an auxiliary radiator to establish a temperature differential between the secondary and primary coolants during startup and also to remove excess heat from the magnetic structure during normal operation (see Figs. 3 and 4).

The configuration of the TE-EM pump assembly chosen for the SP-100 system is shown in Fig. 3. As this figure and Fig. 4 show, the pump circulates the lithium coolant in a pair of secondary and primary loops, and the pump's TE generators, which supply the electric current needed for pump operation, are sandwiched between the primary and secondary coolant ducts. Because the electric voltage produced by the TE generators changes proportionally to the temperature difference across the TE elements, the pump will operate autonomously as long as a temperature difference exists between the primary and secondary coolant loops. Also, by virtue of the temperature dependence of the voltage produced by the TE elements, the pump is self-regulating.

The pump is configured such that the electric current circulating through the ducts induces a magnetic field in the magnetic structure (Hiperco-27) and coolant ducts. Figure 4 illustrates the direction of the current and the magnetic flux through the lithium coolant ducts and the direction of the flow that is produced. The magnetic structure directs the magnetic flux through the lithium coolant ducts perpendicular to the electric current.

Although not insulating the magnetic structure from the secondary coolant ducts reduces the pump mass, it also makes the pump vulnerable to overheating of the secondary coolant. This overheating, occurring as a result of an exposure of the system's radiator to external heating, could degrade the pump operation and result in a loss of flow in the secondary loop. A single or multiple failure of the TE-EM pumps could reduce the flow through the reactor core, causing both the reactor thermal power and the system's electric power to decrease.[5] Therefore, it is important not only to investigate the performance of the dual-loop TE-EM pump during nominal operation but also to assess its reliability under adverse operating conditions.

This research focused on developing a coupled model to simulate the operation of the SP-100 dual-loop TE-EM pump and evaluate its vulnerability to overheating of the secondary coolant. The dual-loop pump model has been incorporated in the latest version of the Space Nuclear Power System Analysis Model (SNPSAM Mode-3), which is being used for performing reliability and survivability analyses of the integrated SP-100 system.[5] This paper presents the results of a parametric analysis investigating the effects of changing the primary and secondary coolant temperatures, insulating the magnetic structure from the secondary coolant ducts, and/or overheating of the secondary coolant on the pump performance during both steady-state and transient operation. The following two sections describe the dual-loop TE-EM pump and the pump model, respectively.

Description of the Dual-Loop TE-EM Pump

Figure 4 presents a cross-sectional view of the dual-loop TE-EM pump, and Fig. 5 presents a line diagram illustrating

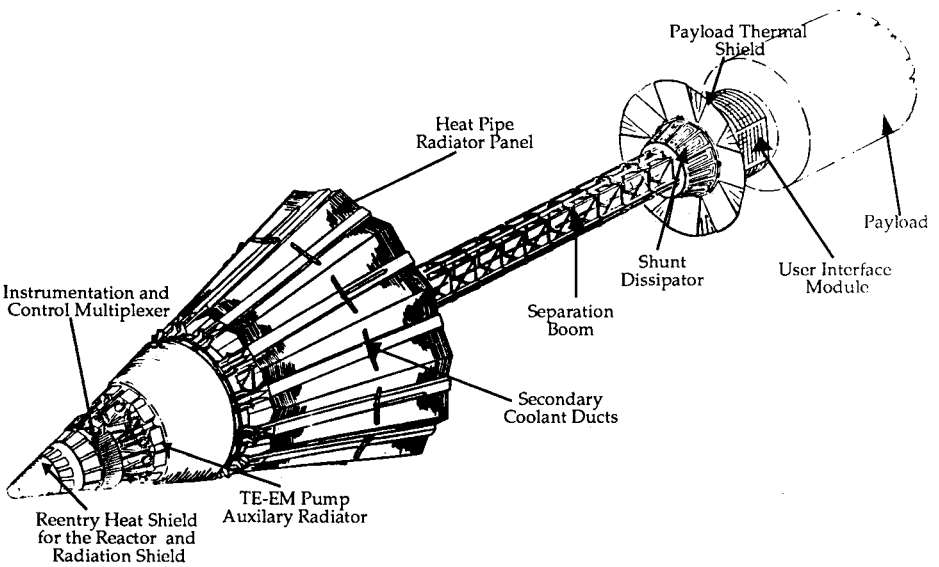

Fig. 1 SP-100 space nuclear power system.

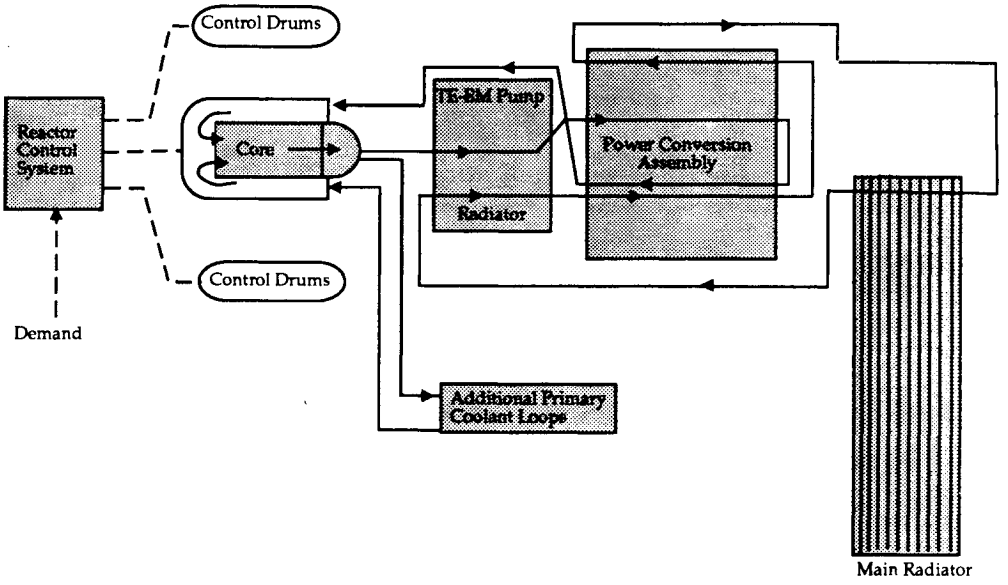

Fig. 2 Schematic of the SP-100 primary and secondary coolant loops in the SP-100 system.

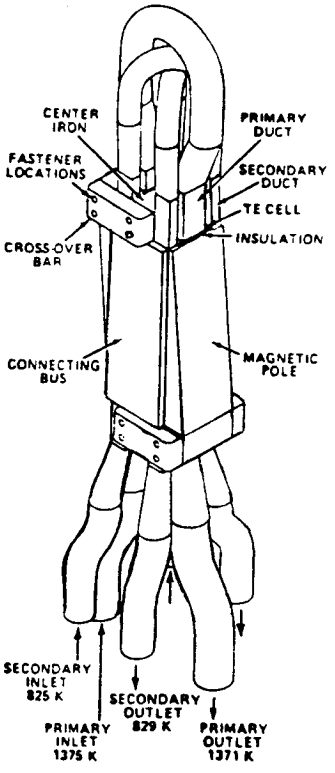

Fig. 3 Configuration of the TE-EM pump assembly for the SP-100 system.

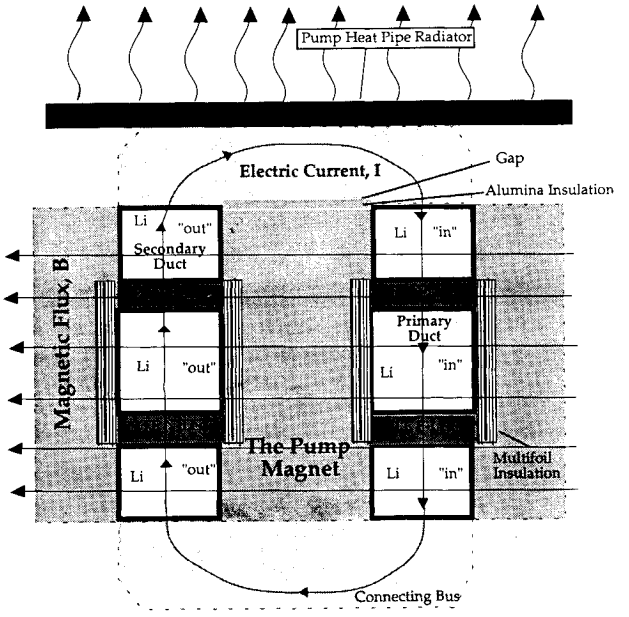

Fig. 4 Cross-sectional view of the dual-loop TE-EM pump.

the pump's operation. As indicated earlier, the pump is equipped with a self-induced Hiperco-27 magnetic structure for providing the magnetic flux and TE generators for supplying the direct current needed for the operation of the pump.

The electromagnetic (EM) pump operates on the Faraday principle, which specifies that a driving force is generated perpendicularly to both the magnetic field and the electric current, which flow at a right angle to each other. As shown in Fig. 3, the primary coolant enters the pump through the middle duct on the right-hand side and exits through the duct on the left-hand side, while the secondary coolant flows through two ducts, one on each side of the primary ducts. The direct current I generated by the TE generators passes through the coolant ducts at a right angle to the magnetic flux B, causing the liquid metal coolant to flow in the perpendicular plane. Details on the theory of the EM pump can be found elsewhere.[6-9]

As illustrated in Fig. 4, the N and P elements of the TE generators are conductively coupled to both the primary and secondary coolant ducts. The temperature differential between the primary and secondary coolants induces electric current in the TE generators by the Seebeck phenomena.[10,11] The nominal values of the primary and secondary coolant temperatures in the SP-100 system are 1350 and 800 K, respectively. The conversion efficiency of the TE generators, which is strongly dependent on the physical properties of the TE materials, generally increases with the temperature differential across the TE converters and the value of the primary coolant temperature. To reduce the electrical losses in the pump, buses with negligible electrical resistance are used for internal electric connections in the pump (see Fig. 4). In addition, the upper bus thermally couples the upper two secondary coolant ducts to the auxiliary radiator of the pump but is electrically insulated from

the magnetic structure by alumina insulation (see Fig. 4). Because the alumina insulation (1.27 cm thick) is separated from both the magnetic structure and the upper bus by small gaps (0.00254 cm each), in the space environment the alumina insulation will be radiatively coupled to the magnetic structure and the bus. The lower bus, however, is thermally insulated from both the coolant ducts and the pump magnetic structure.

Dual-Loop TE-EM Pump Model

The pump model is a dynamically and functionally coupled model that incorporates three submodels: an EM pump model, a quasi-steady-state thermal model of the magnetic structure, and a transient TE generator model.[11] This pump model is similar to that developed for the single loop TE-EM pump,[12] except for the thermal management of the magnetic structure, the thermal coupling of the TE generators to the primary and secondary coolant ducts, and the thermal coupling of the secondary ducts and the magnetic structure to the auxiliary radiator of the pump.

The TE model is described in detail elsewhere[11] and therefore will not be presented here. The TE model is a one-dimensional, transient model that can handle any combination of boundary conditions at the hot and cold ends of the TE elements (see Table 1). The model also incorporates the effects of temperature on the physical properties of the TE materials. These properties include the Seebeck coefficient, thermal and electric conductivities, density, and the specific heat. The governing equation for the TE generators is solved using the finite-element method coupled to a time integration algorithm. The results of the TE model have been verified by comparing the model predictions with the exact solutions for two cases of isothermal and isoflux boundary conditions. The model predictions of the spatial temperature distributions in the N and P elements as well as of the conversion efficiency, the electric current and power output, were in excellent agreement with the exact solutions, within $\pm 1\%$.[11]

The model of the magnetic structure thermally couples the magnetic structure to both the primary and secondary coolant ducts and to the auxiliary radiator of the pump. The model calculates the average temperature of the magnetic structure as a function of the primary and secondary coolant temperatures and the number of insulating foils between either the primary or the secondary coolant ducts and the magnetic structure. Given the nominal value of the magnetic flux strength, the model of the magnetic structure then follows the saturation induction curve of the Hiperco-27 material to determine the magnetic flux density in the coolant ducts as a function of the calculated average temperature of the magnetic structure. For simplicity, the magnetic fluxes in the primary and secondary coolant ducts are assumed to be uniform but differing in value. The effect of the duct shape on the effective magnetic flux value, however, was not modeled because it was beyond the scope of this study. The following sections describe the models of the EM pump and of the magnetic structure.

EM Pump Model

The operation of the TE-EM pump is described by the classic model of Barnes[7] and Blake[8] where the pressure head ΔP developed in the liquid metal coolant as it travels through the pump duct is calculated in terms of the effective current I_e and the magnetic flux B as follows (see Fig. 6):

$$\Delta P = \left(\frac{BI_e}{10^4 b}\right)\left(\frac{R_W R_f}{\bar{R}}\right) - \left(\frac{B^2 Q}{10^8 b^2}\right)\left(\frac{R_W + R_f}{\bar{R}}\right) \tag{1}$$

To give the coolant volumetric flow rate through the pump duct in terms of the pressure head developed across the duct, Eq. (1) can also be rearranged as follows:

$$Q = \left(\frac{10^4 I_e b}{B}\right)\left(\frac{R_W R_f}{R_W + R_f}\right) - \left(\frac{10^8 b^2 \Delta P}{B^2}\right)\left(\frac{\bar{R}}{R_W + R_f}\right) \tag{2}$$

In these equations the resistance $\bar{R}$ is expressed in terms of those of the wall and the coolant and the fringe losses as

$$\bar{R} = R_e R_W + R_e R_f + R_f R_W \tag{3}$$

where the effective resistance of the coolant R_e is determined in terms of the coolant resistance at the operating temperature $r_c(T)$ and the duct geometrical parameters as

$$R_e = \frac{r_c(T)a}{bL} \tag{4}$$

It should be noted that in the SP-100 dual-loop TE-EM pump the width b and the height a of the primary and second-

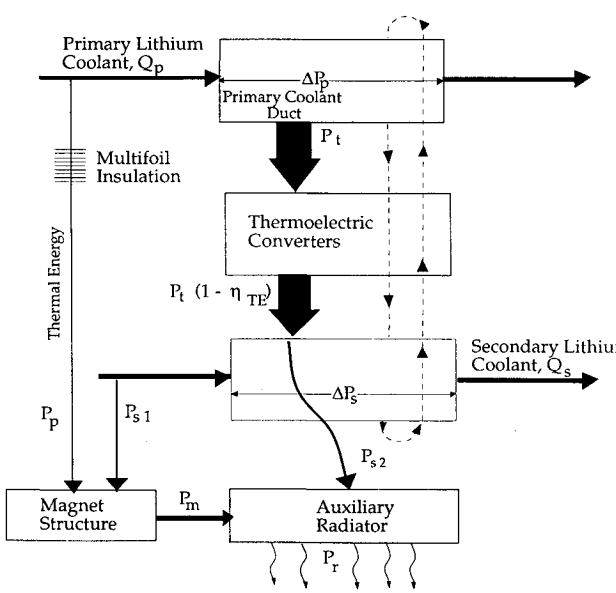

Fig. 5 Flowchart of the operation of the dual-loop TE-EM pump.

Table 1 Boundary condition choices in the transient thermoelectric model

Choice	Hot side	Cold side
I	Constant or time-dependent Temperature	Constant or time-dependent Temperature
II	Heat flux	Same as I
III	Temperature	Radiative cooling
IV	Heat flux	Radiative cooling

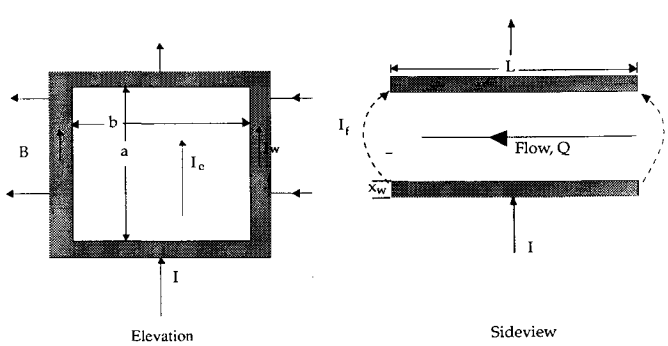

Fig. 6 Schematic of the coolant duct.

ary coolant ducts are different, but that the length L is the same for both ducts. Figure 6, which presents a cross-sectional view of a coolant duct, illustrates the operation of the EM pump, and Fig. 7 shows the equivalent electric circuit of the duct. In Eqs. (1-3) R_W can be determined in terms of the electric resistance of the wall material at the coolant temperature, $r_{wm}(T)$, and the area of the wall at a right angle to the flow of the electric current as

$$R_W = \frac{r_{wm}(T)a}{2Lx_w} \tag{5}$$

In Eq. (5) the electrical resistances due to brazed or welded joints are neglected.

An accurate estimate of the fringe resistance of the coolant, R_f, entails solving a complicated expression incorporating the pump geometry, the magnetic field distribution, and the coolant velocity profile in the pump ducts. However, for simplicity, the fringe resistance is assumed to be equal to 10 times the effective wall resistances R_W.[9,13] From the equivalent electric circuit of the pump duct shown in Fig. 6, the electric potential across the duct can be given as[6-9]

$$E = \frac{BQ}{10^4 b} + \frac{10^4 b R_e \Delta P}{B} + Ir_w \tag{6}$$

where the resistance r_w can be given as

$$r_w = \frac{2r_{wm}(T)x_w}{(b+2x_w)L} \tag{7}$$

The total electric power input to the dual-loop TE-EM pump $P_{e\text{EM}}$ is equal to the sum of those supplied to the secondary and the primary coolant ducts P_p and P_s, thus

$$P_{e\text{EM}} = P_p + P_e \tag{8}$$

where

$$P_p = N_p I E_p \tag{9}$$

$$P_s = N_s I E_s \tag{10}$$

In Eqs. (9) and (10) E_p and E_s are given by Eq. (6) after substituting the geometrical parameter and the coolant flow rates in the primary and secondary ducts, respectively. The EM pump efficiency η_{EM}, defined as the ratio of the mechanical power developed in the pump P_M to the electric power supplied by the TE generators, is

$$\eta_{\text{EM}} = \frac{P_M}{P_{e\text{EM}}} = \frac{(N_p Q_p \Delta P_p + N_s Q_s \Delta P_s)}{2P_{e\text{EM}}} \tag{11}$$

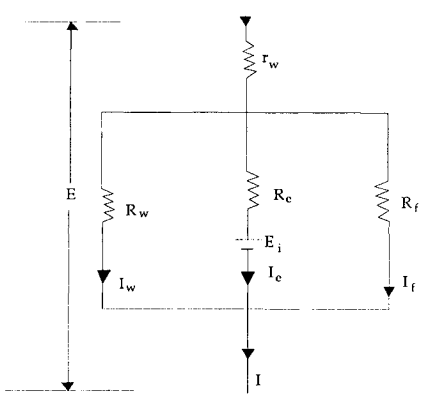

Fig. 7 An equivalent circuit of the pump duct.

Subsequently, the overall efficiency of the dual-loop TE-EM pump $\eta_{\text{TE-EM}}$ can be given as the product of four quantities:

$$\eta_{\text{TE-EM}} = \eta_{\text{EM}}\eta_{\text{TE}}\eta_t\eta_e \tag{12}$$

While the TE conversion efficiency η_{TE}, defined as the ratio of the electric power produced by the TE generators $P_{e\text{TE}}$ to the thermal power supplied by the primary coolant P_t, is calculated directly by the TE model, the other two efficiencies are calculated as follows:

$$\eta_t = \frac{1}{1+[(P_m + P_{\text{losses}})/P_t]} \tag{13}$$

$$\eta_e = \frac{P_{e\text{EM}}}{P_{e\text{TE}}} \tag{14}$$

In Eq. (13), P_m and P_{losses} are the thermal losses to the magnetic structure by conduction from the primary and secondary coolant ducts, as well as the loss to the auxiliary radiator by conduction from the top two secondary ducts, respectively, (see Fig. 5). While the latter can be neglected during the pump's normal operation, it could be important at higher secondary coolant temperatures. These losses are calculated by the thermal model of the magnet, which is described in the following section.

Magnet Thermal Model

During nominal operation the temperature of the magnetic structure material (Hiperco-27) is kept well below its Curie point temperature of approximately 1240 K; above this temperature the magnetic material becomes paramagnetic and the pump ceases to operate. At temperatures below the Curie point of Hiperco-27, the magnetic flux density is a strong function of temperature, decreasing as the magnet temperature increases.[12] Therefore, it is important to determine the magnetic field strength as a function of the average magnet temperature, to model accurately the operation of the TE-EM pump, and hence of the operation of the integrated SP-100 system.[5]

For example, a reduction in the reactor's thermal power decreases the primary coolant temperature, lowering the magnet's temperature and increasing the magnetic field strength. Conversely, decreasing the primary coolant temperature re-

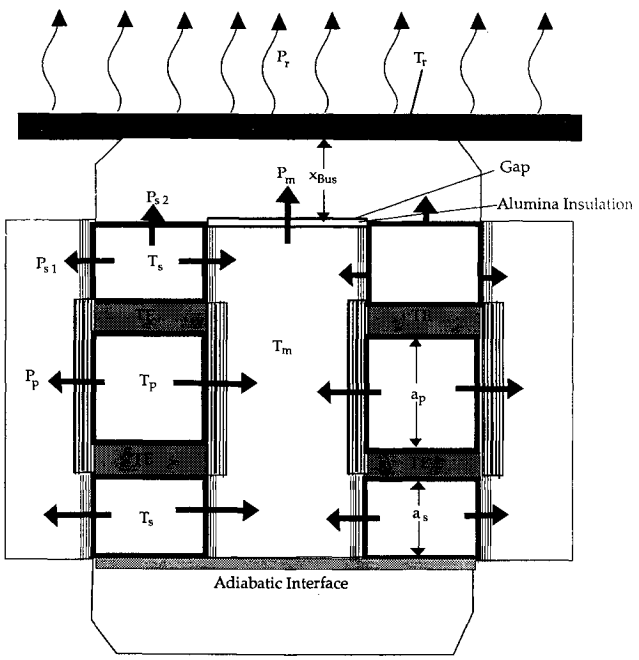

Fig. 8 Pump magnet thermal model diagram.

duces the electric current supplied by the TE generators, hence reducing the magnetic field strength. Although both effects are important in determining the effective magnetic field strength in the coolant ducts, the latter is more pronounced. Also, a rise in the secondary coolant temperature due to an external thermal exposure of the SP-100 radiators reduces the temperature difference across the TE generators, and hence the electric current and magnetic field. At the same time higher secondary temperatures could cause the temperature of the magnetic structure to increase, reducing the magnetic field strength and degrading the pump's performance.

Because the Curie point of Hiperco-27 is significantly higher than the nominal temperature of the secondary coolant (800 K) but lower than that of the primary coolant (1350 K), the magnetic structure is thermally insulated only from the primary coolant ducts. This insulation consists of very low effective thermal conductivity multifoils (see Fig. 4). However, the magnet thermal model allows for insulating the magnet structure from the secondary ducts to investigate the effects on pump performance during both normal and adverse conditions (see Fig. 8).

The magnet thermal model calculates the average magnet temperature as a function of the temperatures of the primary and secondary coolants and the number of the insulation foils between the magnet structure and either the primary or the secondary coolant ducts. The calculated average magnet temperature is then used to determine the magnetic field strength.[12] Also, the coupling of the TE generator model to the EM pump model allowed for the inclusion of the effect of varying the electric current on the magnetic flux strength, assuming a linear relationship.[14]

Figure 8 presents a schematic diagram of the magnet thermal model with the appropriate notation and the boundary conditions. As Fig. 8 shows, the lower boundary between both the magnetic structure and the secondary coolant ducts and the connecting bus is adiabatic. However, at the upper boundary the magnetic structure is radiatively coupled and the secondary ducts are conductively coupled to the auxiliary radiator. Because of the high thermal conductivity and the small thickness of the coolant duct walls, the wall temperature is assumed uniform and equal to the average magnet temperature. Similarly, the interface temperature between the upper electric bus and the secondary ducts is assumed uniform and equal to the average magnet temperature but different from the radiator temperature T_r. The axial conduction in the multifoil region isneglected, confining the flow of heat in the foils to the perpendicular direction. This assumption is justified because the thickness of the insulation foil (0.005 cm) is much smaller than its length (3.7 cm for the primary duct). Finally, for simplicity, the temperature distribution in the bus is assumed to be linear during the transient operation of the pump because of the small thickness and relatively small mass of the upper electric bus compared to that of the pump magnetic structure.

The overall transient heat balance of the magnetic structure can be written as

$$P_s + P_p - P_m = M_m Cp_m \frac{\partial T_m}{\partial t} \tag{15}$$

where

$$P_s = 2N_s h_{s1} A_{s1} (T_s - T_m) \tag{16}$$

$$P_p = 2N_p h_p A_p (T_p - T_m) \tag{17}$$

$$P_m = h_m A_m (T_m - T_r) \tag{18}$$

In Eqs. (15–18) the heat-transfer coefficients are given as

$$h_{s1} = \left[\frac{1}{h_s} + \frac{x_w}{k_w} + \frac{x_{\text{foil}}}{k_{\text{foil}}} \right]^{-1} \tag{19}$$

$$h_{p1} = \left[\frac{1}{h_p} + \frac{x_w}{k_w} + \frac{x_{\text{foil}}}{k_{\text{foil}}} \right]^{-1} \tag{20}$$

$$h_m = \left[\frac{x_B}{k_B} + \frac{x_{Al}}{k_{Al}} + \frac{1}{h_{g1}} + \frac{1}{h_{g2}} \right]^{-1} \tag{21}$$

In Eq. (21) the conductance of the gap is given by[15]

$$h_g = \frac{4\sigma T_{\text{av}}^3}{\left(\frac{1}{\epsilon_{Al}} + \frac{1}{\epsilon_i} - 1 \right)} \tag{22}$$

The convective heat-transfer coefficients h_s and h_p are calculated using the following relation[16]:

$$h_c = k_c / [D_e (5.8 + 0.02 Pe^{0.8})] \tag{23}$$

where the Peclet number is given as

$$Pe = \rho_c Q_c / (A_c Cp_c k_c) \tag{24}$$

The physical properties in Eqs. (23) and (24) are evaluated at the bulk temperature of the lithium coolant, and the effective conductivity of the multifoil insulation is calculated as a function of the average temperature of the magnetic structure, the number of foils, foil thickness, coolant temperature, and effective thermal conductivity of the foil material as follows[12]:

$$k_f = 4 x_{\text{foil}} \epsilon_f \sigma (T_m + T_c)(T_m^2 + T_c^2)/(N_{\text{foil}} + 1) \tag{25}$$

The heat balance for the auxiliary radiator of the pump can be approximated as

$$h_r A_r (T_r - T_a) = \tfrac{1}{2} N_s h_{s2} A_{s2} (T_s - T_r) + h_m A_m (T_m - T_r) \tag{26}$$

In this equation, the first and second terms on the left-hand side represent, respectively, the heat flow from the upper two secondary ducts to the auxiliary radiator and the heat flow from the magnetic structure to the radiator. In Eq. (26), the overall heat-transfer coefficients for the secondary duct and the auxiliary radiator are given as

$$h_{s2} = h_B + \left[\frac{1}{h_s} + \frac{x_w}{k_w} \right]^{-1} \tag{27}$$

$$h_r = \epsilon_r \sigma F_r (T_r^2 + T_a^2)(T_r + T_a) \tag{28}$$

Equations (15) and (26) are solved analytically to yield the following expression of the transient mass-averaged temperature of the magnetic structure:

$$T_m(t) \cong \left(\frac{H_2}{H_1} \right) + \left[T_m(t_\phi) - \left(\frac{H_2}{H_1} \right) \right] e^{-\frac{H_1 t}{M_m Cp_m}} \tag{29}$$

where $T_m(t_\phi)$ is the average magnet temperature at the beginning of the transient. The coefficients H_1 and H_2 are given as

$$H_1 = (2N_s h_{s1} A_{s1} + 2N_p h_p A_p + h_B A_B) \tag{30}$$

and

$$H_2 = (2N_s h_{s1} A_{s1} T_s + 2N_p h_p A_p T_p + h_B A_B T_r) \tag{31}$$

In these equations, while the initial temperatures of the primary and secondary coolants T_s and T_p are known for a given transient, the radiator temperature is calculated by the relation

$$T_r = \left[\frac{(\tfrac{1}{2} N_s h_{s2} A_{s2}) T_s + h_B A_B T_m + h_r A_r T_a}{\tfrac{1}{2} N_s h_{s2} A_{s2} + h_B A_B + h_r A_r} \right] \tag{32}$$

During the transient operation of the pump, Eqs. (29) and (32) are solved simultaneously to determine the average magnet temperature and the temperature of the auxiliary radiator as function of time. However, for steady-state operation Eq. (32) remains the same, while Eq. (29) is reduced to

$$T_m = \left(\frac{H_2}{H_1}\right) \tag{33}$$

As indicated earlier, the physical properties of the duct wall materials, the Hiperco-27, and those of the primary and secondary coolants are allowed to change with temperature.

The magnet thermal model is coupled to both the EM pump model described in the previous section and the transient model of the TE generator.[11] The integrated TE-EM pump model is used to investigate the performance of the pump during both steady-state and transient operation. The results of this investigation and those of the parametric analysis assessing the effect of changing the secondary and primary coolant temperatures and the number of insulating foils between the coolant ducts and the magnet structure are presented and discussed in the next section.

Results and Discussion

This section presents the results of the parametric and reliability analyses of the SP-100 dual-loop TE-EM pump. Table 2 lists the design parameters for the pump and the values of the nominal base-case operating conditions. Two sets of analyses were performed: 1) a parametric, steady-state analysis of the effect of changing the primary coolant temperature and/or overheating the secondary coolant on the steady-state operation of the pump, also investigating the effect of insulating the magnetic structure from the secondary coolant ducts on pump performance, and 2) a transient analysis investigating the response and vulnerability of the pump to a stepwise increase of the secondary coolant temperature. The results for the steady-state and transient analyses are presented and discussed sequentially in the next two sections.

Table 2 Dual-loop TE-EM pump design and base-case operating parameters

Overall pump dimensions:	
Duct width	1.784 cm
Primary duct height	2.676 cm
Secondary duct height	1.157 cm
Duct wall thickness	
Primary	0.076 cm
Secondary	0.040 cm
Duct wall materials	
Primary	PWC-11
Secondary	Ti
Active pump length	25.5 cm
Primary coolant temperature	1350 K
Secondary coolant temperature	800 K
Primary mass flow rate	1.0 kg/s
Secondary mass flow rate	1.0 kg/s
Thickness of the electric bus	0.764 cm
Electric bus material	Cu
Pump magnet dimensions:	
Magnet height	7.41 cm
Magnet width	3.148 cm
Magnet material	Hiperco-27
Area of the radiator	0.138 m^2
Magnet mass	10.5 kg
Nominal magnetic flux	
Primary	572 G
Secondary	650 G
Magnet Curie point	1240 K
Thermoelectric parameters:	
TE material	SiGe/GaP
TE length	0.3 cm
Number of foil insulations	
Primary duct	30
Secondary duct	None
Thickness of foil insulation region	0.3 cm
Foil thickness	0.005 cm
Auxiliary radiator area	0.1413 m^2

Steady-State Operation and Reliability Analysis

Figures 9–14 present the results of the parametric analysis focusing on the steady-state operation and the reliability of the SP-100 dual-loop TE-EM pump. Because the top two secondary coolant ducts in the pump are conductively coupled to both the magnetic structure and the auxiliary radiator, the average magnet temperature, and hence the magnetic flux strength, are sensitive to changing the temperature of the secondary coolant (see Fig. 9). This sensitivity results because increasing the secondary coolant temperature not only increases the heat flow from the secondary duct to the magnetic structure but also increases the radiator temperature, resulting in a higher magnet temperature. In addition, changing the secondary coolant temperature changes the electric current provided by the TE generators and hence the magnetic field strength in the coolant ducts. As shown in Fig. 9, a 50% increase in the secondary coolant temperature, above that of the base case (from 800 to 1200 K), causes the average magnet temperature to increase by almost the same percentage (from 798 to 1191 K). Also, Fig. 9 demonstrates that using only five foils to insulate the magnet structure from the secondary ducts effectively reduces the average magnet temperature, and hence increases the pump head (see Fig. 10). As delineated in Figs. 9 and 10, this reduction in the magnet temperature not only improves the pump performance but also allows the pump to operate at secondary coolant temperatures 90 K higher than that of the base case (1255 K) before a loss of flow occurs. Beyond secondary coolant temperatures of 1255 and 1345 K for the uninsulated and insulated secondary ducts, respectively, the pump ceases to operate because the average magnet temperature exceeds the Curie point of the magnet material (1240 K) (see Fig. 12).

As shown in Fig. 10, using more than five foils to insulate the magnet from the secondary ducts insignificantly affects the pump performance. However, the loss in the pump pressure head increases as the secondary coolant temperature increases. For example, in the insulated secondary ducts case increasing the secondary coolant temperature from 1200 to 1300 K, while keeping the primary coolant temperature at 1350 K, reduces the primary pump head from 5.8% to as low as 0.4% of the nominal value for the base case. In Fig. 10 the induced pump head in the secondary coolant is slightly higher than that in the primary coolant because the effective magnetic flux density in

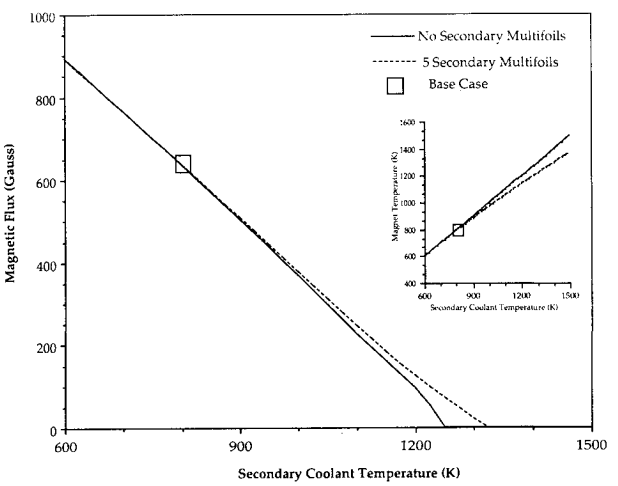

Fig. 9 Effect on pump performance of changing the secondary coolant temperature.

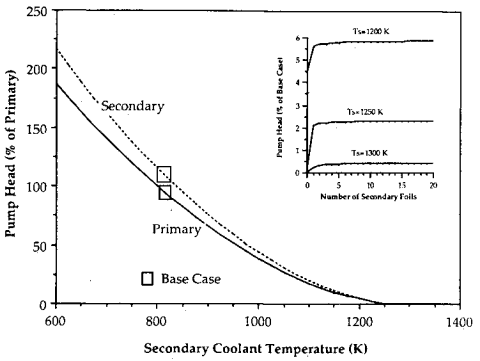

Fig. 10 Effect of varying the secondary coolant temperature and insulating the secondary ducts on the steady-state operation of the pump.

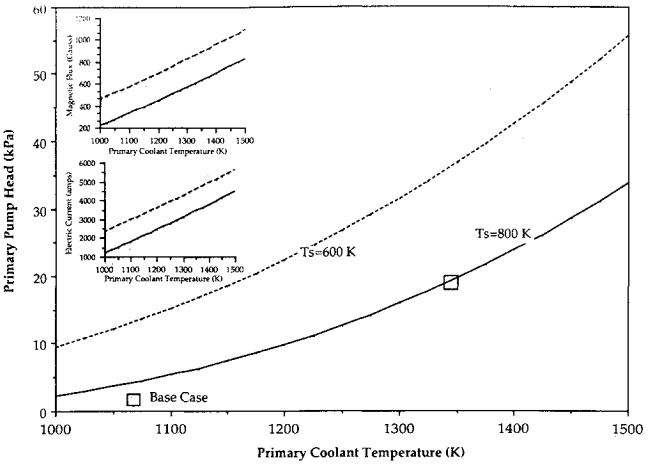

Fig. 11 Effect of varying the primary coolant temperature on the steady-state operation of the SP-100 pump.

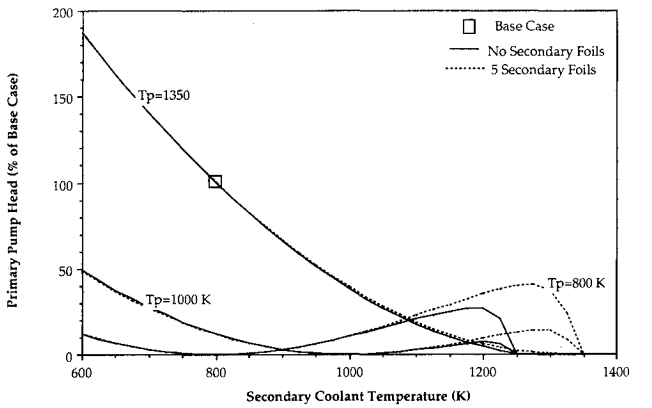

Fig. 12 Effect of varying the primary coolant temperature and overheating the secondary coolant on the SP-100 pump steady-state operation.

the secondary ducts is higher than that in the primary ducts (see Table 2).

Figure 11 shows that increasing the temperature differential between the primary and secondary coolants ΔT increases the electric current produced by the TE generators and hence the magnetic field strength, thus enhancing pump performance. As demonstrated in Fig. 11, while the electric current increases linearly with ΔT, the primary pump head increases proportionally to ΔT^2. This figure also shows that increasing the temperature differential across the TE generators by increasing the primary coolant temperature induces a pump head slightly higher than that obtained by raising the secondary coolant temperature by the same amount. For example, a 200 K increase in ΔT by raising the primary coolant temperature from 1100 to 1300 K or lowering the secondary coolant temperature from 800 to 600 K increases the primary pump head by 284 and 299%, respectively.

The results delineated in Fig. 12 show that for a primary coolant temperature lower than that of the base case (1000 K) a loss of flow condition in the secondary coolant ducts of the SP-100 TE-EM pump could be caused by two mechanisms. The first mechanism is the loss of the TE electric current, and the second is the loss of magnetic flux. As Fig. 12 indicates, when the secondary coolant temperature becomes equal to the primary coolant temperature, the pump ceases to operate due to loss of electric current. A further increase of the secondary coolant temperature beyond that of the primary coolant establishes a temperature gradient in the TE generators but in reverse, causing both the electric current and magnetic field to reverse direction. In this case the pump resumes its operation, where the pump head increases as the secondary coolant tem perature increases. However, increasing the secondary coolant temperature increases the electric current produced by the TE generators and hence the magnetic flux density, but also increases the average magnet temperature, causing the magnetic-field strength in the pump ducts to decrease. As shown in Fig. 12, when the increase in the pump head due to higher electric current equals the decrease caused by the lower magnetic flux, the pump head reaches a peak. Beyond this point, increasing the secondary coolant temperature causes the magnetic field strength to decrease faster than the increasing electric current, resulting in a lower pump head. Eventually, a second loss of flow will occur as the average magnet temperature becomes equal to the Curie point of the magnet material (1240 K).

It is worth noting that the results shown in Fig. 12 demonstrate that in the base case at secondary coolant temperatures beyond 1000 K, the primary pump head for the insulated secondary duct case is only slightly higher than that for the uninsulated case. However, the difference in pump head between the insulated and uninsulated cases becomes significant as the primary coolant temperature decreases below the nominal value for the base case (1350 K).

Had the pump been designed with a permanent magnet rather than with a self-induced one, not only would the magnet mass have been larger, but also raising the secondary coolant temperature beyond that of the primary coolant would have caused the pump to operate in reverse (see Fig. 13). The reverse operation is because reversing the temperature differential across the TE generators would only reverse the direction of the electric current in the coolant ducts. In Fig. 13, because the mass flow rate is kept constant (see Table 2), the calculated pump head is not zero. However, in the actual system where the pump is coupled to other system components, a loss of electric current will cause not only the flow rate but also the pump head to be zero.

The various operating regimes of the SP-100 dual-loop TE-EM pump under steady-state conditions are shown in Fig. 14. As this figure indicates, for a secondary coolant temperature higher than 1255 K, the pump produces no pressure head. However, insulating the magnet structure from the secondary ducts using only five insulating foils raises this temperature to 1345 K. Results in Fig. 14 demonstrate that insulating the pump magnet from the secondary coolant ducts also increases the primary coolant temperature at which a loss of flow occurs. Figure 14 also shows that the pump always operate in forward when either the primary coolant temperature is higher than the secondary coolant temperature or when the latter is higher than the former.

The next section presents and discusses the results of the analysis investigating the transient response and operating parameters of the SP-100 dual-loop TE-EM pump following a stepwise increase in the secondary coolant temperature. The results of the analysis could be useful in assessing the vulnerability of the TE-EM pump to a directed energy threat to the SP-100 radiator.

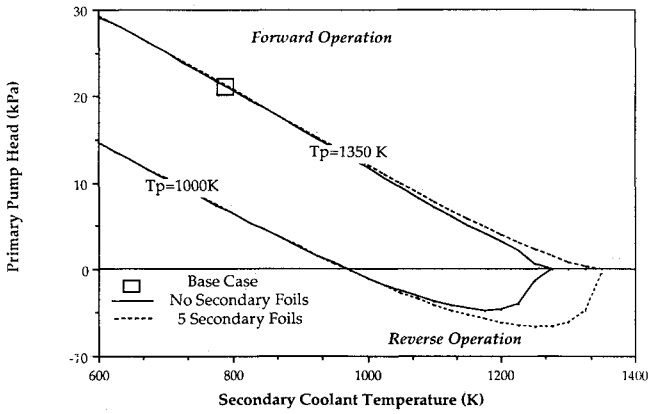

Fig. 13 Steady-state operating regimes of a dual-loop TE-EM pump with a permanent magnet.

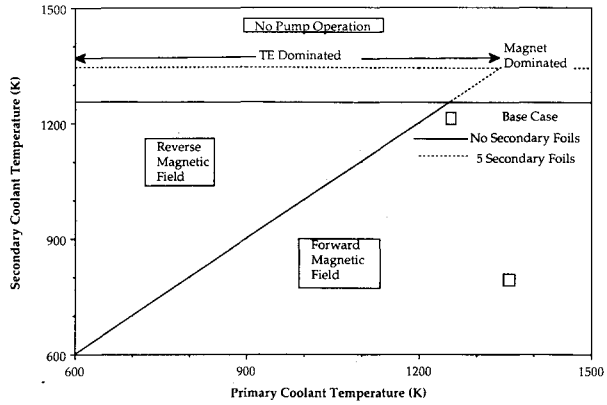

Fig. 14 Steady-state operating regimes of the SP-100 dual-loop pump with a self-induced magnet.

Transient Operation and Reliability Analysis

Figures 15–17 present the results of the transient response of the SP-100 dual-loop TE-EM pump to a stepwise increase in secondary coolant temperature. As Figs. 15 and 16 demonstrate, while a stepwise rise in the secondary coolant temperature results in a stepwise decrease in the electric current, it causes slower changes in the other parameters affecting pump performance. In general, a rise in the secondary coolant temperature causes the pump head and efficiency to decrease, due to the induced reduction in both the magnetic flux and the electric current. As shown in these figures, as soon as the external heating is removed, causing the secondary coolant temperature to return to its initial value, the pump recovers its normal operation, but with a delay time. Figures 15 and 16 indicate that insulating the secondary coolant ducts significantly reduces the peak temperature of the magnet and hence the pump's vulnerability. For example, Fig. 15 shows that insulating the secondary ducts decreases the peak magnet temperature from 999 to 862 K and limits the maximum decline in the pump head to 38 rather than 42% for the uninsulated case.

When the peak secondary coolant temperature was 1300 instead of 1000 K, insulating the secondary coolant ducts prevented the occurrence of a loss of flow, which otherwise occurs if the secondary coolant ducts are not insulated (see Fig. 16). The results plotted in Fig. 16 indicate that a stepwise increase in the secondary coolant temperature from 800 to 1300 K triggers a loss of flow due to the lack of magnetic flux caused by overheating the magnetic structure above its Curie point of 1240 K. However, insulating the secondary ducts from the magnet structure with only five foils precludes the occurrence of the loss of flow; instead, the primary pump head declines to 0.9% of its initial value. Figure 16 also shows that for uninsulated secondary ducts (base case) a loss of flow occurs after 15 s following the increase in secondary coolant temperature. A comparison of the results in Figs. 15 and 16 shows that the

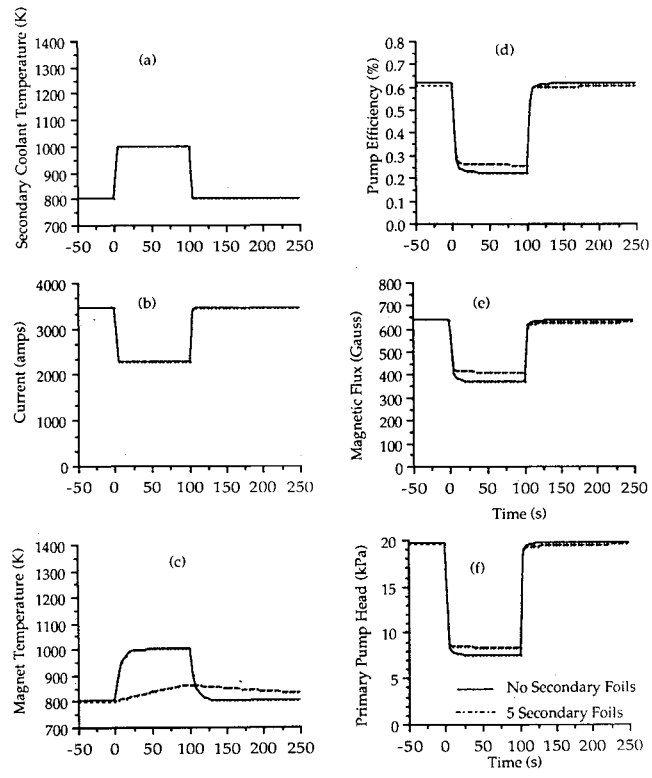

Fig. 15 Transient response of the SP-100 dual-loop TE-EM pump to a stepwise rise in secondary coolant temperature to 1000 K.

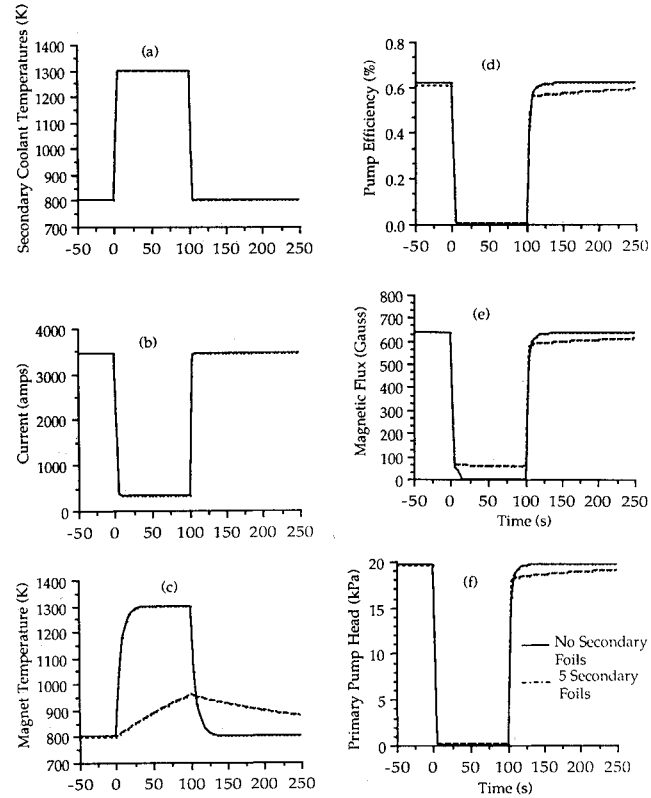

Fig. 16 Transient response of the SP-100 dual-loop TE-EM pump to a stepwise rise in the secondary coolant temperature to 1350 K.

peak magnet temperature increases with the peak value of the secondary coolant temperature. For example, when the secondary ducts are insulated, the peak magnet temperature increases from 862 to 960 K for peak secondary coolant temperatures of 1000 and 1300 K, respectively.

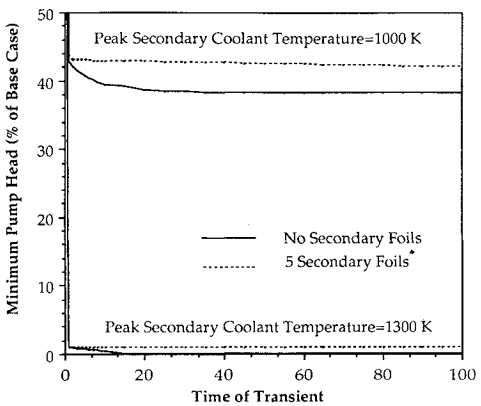

Fig. 17 Effect of the transient time on the SP-100 dual-loop pump response to a stepwise rise in the secondary coolant temperature.

Results show that the vulnerability of the dual-loop TE-EM pump depends not only on the peak value of the secondary coolant temperature but also on the time of the transient. As delineated in Fig. 17, the pump head decreases rapidly with the time of the transient, up to approximately 5 s. Beyond this time the minimum pump head becomes almost independent of the time of the transient but decreases as the peak secondary coolant temperature increases. Figure 17 also delineates the effects of insulating the magnet structure from the secondary coolant duct on the transient operation of the pump. In every case, insulating the pump magnet from the secondary coolant ducts positively impacts the transient performance of the pump.

Summary and Conclusions

This research developed a transient model of the dual-loop TE-EM pump of the SP-100 system and investigated the effects of overheating the secondary coolant on the reliability and vulnerability of the pump. Results show that overheating the secondary coolant could cause a loss of flow in the secondary coolant loops in two cases: when the temperature differential across the TE generators in the pump becomes zero, and when the pump magnet is overheated beyond the Curie point of the magnet material. Results also show that although insulating the pump magnet from the secondary coolant ducts insignificantly affects the nominal steady-state operation of the pump, using only five foils to insulate the magnet not only improves pump performance but also reduces its vulnerability and enhances its reliability at higher secondary coolant temperatures. Analysis shows that insulating the magnet structure from the secondary ducts also minimizes the impact on pump operation of stepwise increases in the secondary coolant temperature. However, the recovery time of the pump increases as the peak value of the secondary coolant temperature increases and/or the magnet structure is insulated from the secondary coolant ducts.

These results suggest that the magnet structure in the dual-loop TE-EM pump should be insulated from the secondary ducts in order to improve the reliability and survivability of the pump to directed energy threats that overheat the secondary coolant. Results also indicate that operating the SP-100 system at high power, although it increases the primary coolant temperature, would reduce the impact of an external threat on the operation of the TE-EM pump.

Results show that the SP-100 pump, which employs a self-induced magnet, will always operate in forward when either the primary coolant temperature is higher than the secondary coolant temperature or when the latter is higher than the former. However, had the pump been designed with a permanent magnet, raising the secondary coolant temperature beyond that of the primary coolant temperature could have caused the pump to operate in reverse.

Acknowledgment

This research is sponsored by the University of New Mexico Institute for Space Nuclear Power Studies.

References

[1]Wright, W., "Accomplishments and Plans of the SP-100 Program," *Space Nuclear Power Systems 1984,* CONF-840113, edited by M.S. El-Genk and M.D. Hoover, Orbit, Malabar, FL, 1985, pp. 37–40.

[2]*SP-100 Conceptual Design Study, Final Report, Volume II—Reactor and Shield Design,* General Electric Co., Philadelphia, PA, 83SDS4261, 1983.

[3]El-Genk, M. S., Seo, J. T., Buksa, J. J., Lapin, S. N., and Evans, B., "Space Nuclear Power System Analysis Model: SNPSAM-Mode 1 and Mode 2," Univ. of New Mexico, Albuquerque NM, Rept. NE-126(88) AFWL-443-1, May 1988.

[4]El-Genk, M. S. and Seo, J. T., "SNPSAM—Space Nuclear Power System Analysis Model, Air Force Weapons Laboratory Report," Kirtland Air Force Base, NM, AFWL-TR-87-36, April 1988.

[5]Rider, W. J., and El-Genk, M. S., "Reliability Studies of SP-100 Class Systems," *Transactions 6th Symposium on Space Nuclear Power Systems,* CONF-89000-Summs, Institute for Space Power Studies, Univ. of New Mexico, Albuquerque, NM, 9-12 January 1989.

[6]Barnes, A. H., "Direct Current Electromagnetic Pumps," *Nucleonics,* Vol. 11, No. 1, 1953, pp. 16–21.

[7]Barnes, A. H., and Cage, J. F., Jr., "Pumps—Electromagnetic, Liquid-Metals Handbook, Sodium NaK Supplement," edited by C. B. Jackson, Bureau of Ships, Dept. of the Navy, Washington, D. C., 1955.

[8]Blake, L. R., "Conduction and Induction Pumps for Liquid Metals," Paper 2111 U, 104(A), *Proceedings of the IEE*, Institute of Electrical Engineering, 1958, pp. 49–63.

[9]Watt, D. A., "The Design of Electromagnetic Pump for Liquid Metals," Paper 2763 U, *Proceedings of IEE*, Institute of Electrical Engineering, 1958, pp. 94–103.

[10]Angrist, W., *Direct Energy Conversion,* Allyn and Bacon, Inc. Boston, MA, 1968.

[11]El-Genk, M. S., and Seo, J. T., "Analysis of Transient Behavior of Thermoelectric Generators in Space Nuclear Power Systems," *Space Nuclear Power Systems 1986,* CONF-860102, edited by M. S. El-Genk and M. Hoover, Orbit, Malabar, FL, 1987, pp. 187–198.

[12]El-Genk, M. S., Buksa, J. J., and Seo, J. T., "A Self Induced Thermoelectric Electromagnetic Pump Model for SP-100 Systems," *Space Nuclear Power Systems 1987,* CONF-860102, edited by M. S. El-Genk and M. D. Hoover, Orbit, Malabar, FL, 1987, pp. 161–172.

[13]Hughes, W. F. and McNab, I. R., "A Quasi-One Dimensional Analysis of an Electromagnetic Pump Including End Effects," *Liquid Metal Flows and Magnohydrodynamics,* Vol. 84, Progress in Astronautics and Aeronautics, AIAA, New York, 1983, pp. 287–312.

[14]Sinha, U., personal communications, General Electric Co., Nov. 1988.

[15]Olander, D. R., *Fundamental Aspects of Nuclear Reactor Fuel Elements,* Technical Information Center, U.S. Dept. of Energy, TID-26711-P1, 1976, Chapter 10, p. 137.

[16]El-Wakil, M. M., *Nuclear Heat Transport,* American Nuclear Society, La Grange Park, IL, 1971, pp. 267–288.